DATING THE FRACTURES IN DARLINGTON ENDPLATES FROM OXIDE THICKNESS MEASUREMENTS

V.F. URBANIC AND M.A. MAGUIRE

AECL Research, Chalk River Laboratories
Chalk River Laboratories
Chalk River, Ontario, Canada K0J 1J0

N. RAMASUBRAMANIAN

Ontario Hydro Research Division
800 Kipling Avenue
Toronto, Ontario, Canada, M8Z 5S4

ABSTRACT

Corrosion film thicknesses on fuel bundle endplates from DNGS Unit #2 were measured using infrared interferometry. Measurements were done on both normal and fracture faces. Regions on fracture faces were smooth enough to provide well-defined spectra. The kinetic equation for oxide growth was established from average thicknesses measured on out-of-flux upstream and downstream endplates. Oxide growth curves calculated using the kinetic equation facilitated estimation of fracture times.

OXIDE THICKNESS MEASUREMENTS

1. INTRODUCTION

The endplates on fuel bundles discharged from Darlington Unit 2 have been exposed to the hot pressurized coolant for about a year. Corrosion film thicknesses on the endplates are expected to be typically pre-transition, up to about 2 μm thick. Dating the fractures may be accomplished by comparing corrosion film thicknesses grown on fracture and normal, unfractured, surfaces. Infrared interferometry is ideally suited as the technique for thickness measurements for the following reasons, viz., it is nondestructive and noncontacting, has a high precision and accuracy and can be used in the microanalysis mode for measurements on small areas (1). The technique to obtain oxide thickness measurements on fatigue-cracked specimens tested in the laboratory and on DNGS endplates, the procedure adapted for dating calculations and the associated fracture times obtained, are presented here.

2. EXPERIMENTAL

A Bio-Rad FTS-40, Fourier Transform InfraRed (FTIR), spectrometer with a 300 UMA microscope and a narrow band Mercury-Cadmium-

Telluride detector was used. A spot 0.3 mm in diameter is illuminated on the specimen surface by the incident infrared beam. A cassegrain lens system used to focus the beam gave a maximum angle of incidence of 25 degrees. The reflected beam is passed through an iris type aperture to the detector and spectra were recorded with the aperture set at 0.1 mm. Measurements were thus possible at a number of locations on a surface. Generally, measurements were made at several locations on the fracture surface and on normal surface at locations close to the fracture surface.

For a film thickness "t", the wavelength "λ" at which an interference peak of an order "n" occurs is given by the equation:

$$2\eta t\cos\phi' + f(\lambda) = (2n-1)\lambda/2$$

where "η" is the refractive index of the corrosion film, "ϕ'" the angle of refraction and "$f(\lambda)$" is the phase shift correction. Both the refractive index and phase shift are functions of wavelength and these are unknown for the corrosion films. An absolute determination of thickness is thus rendered impossible and a calibration procedure is used instead.

Corrosion films of known thicknesses were produced by exposing Zircaloy-4 fuel cladding specimens to lithiated heavy water at 360°C. Specimens were withdrawn at predetermined times and from the weight gained per unit area, film thicknesses were calculated assuming the density of zirconia to be 5.72 (2). Thin films, <0.5 μm thick, were prepared by anodizing at constant applied voltages in 1 wt% potassium hydroxide. A film forming efficiency of 2.9 nm per volt was used to estimate thicknesses (3). The spectral data of these corrosion standards were analyzed and the basis for estimating thicknesses on other specimens was established.

3. RESULTS

3.1 Calibration Standards

A set of spectra for some of the corrosion standards is shown in Figure 1. The numbering of the peaks in each spectrum refers to the order of interference. The number of peaks and their positions in a spectrum are uniquely related to the oxide thickness as defined by the interference equation. Calibration curves (thicknesses plotted against the wavelengths of the interference peaks for various orders) for the standards are shown in Figure 2. A linear relation is seen, the blocked area in the figure, for pre-transition oxides. Extrapolation of the linear portions gives negligibly small values of thickness as the intercept. The slopes of the linear portions correspond to a

value of 2 for the refractive index of the films. In terms of the interference equation the implications are that in the region of wavelengths 2 to 5.5 μm, (i) the refractive index of the oxide is nearly invariant and (ii) thickness correction (related to the intercepts in Figure 2) from different phase shifts at the two interfaces is negligible. For pretransition films, 0.5 to 2 μm thick, the thicknesses can be estimated from:

$$t = (2n-1)\lambda/7.84$$

for interference peaks in the region of wavelengths 2 to 5.5 μm. When more than one order of interference is observed, for example in the case of films 0.8 to 2 microns thick, the second order peak is more reliable for thickness estimates because its position is least affected by absorption effects in the oxide.

In Figure 2, a slight spread is shown in the wavelength at which interference peaks of an order occur for each standard. These spreads represent the variations observed amongst eight to ten measurements on each standard. In terms of thickness, they correspond to variations over the specimen area of ±5% of the gravimetrically measured values. Interferometry is a more precise technique than gravimetry and these variations are real representing small changes in thickness over different areas of a specimen. The thickness derived from weight gain measurements is thus an average of the thicknesses indicated by interferometry. Variations on the order of ±5% in thicknesses measured interferometrically on a surface do not reflect a kinetic significance, i.e., the oxide growth corresponds to a single exposure time.

3.2 **Laboratory Tests**

Endcap/endplate weld specimens, fatigue tested at room temperature to produce incipient cracks, were corroded in lithiated water at 300°C for various times up to 182 d. The extent of the cracks varied from 30 to 90% of the plate thickness. A few specimens were tested under dynamic conditions; these were fatigued in situ during corrosion. Following a corrosion exposure an incipient crack was opened and thickness measurements were made at several locations on the normal and fracture surfaces. The kinetics of oxide growth was followed by examining the specimens after various exposure times.

Spectra obtained for the normal surfaces were of excellent quality, similar to those of the corrosion standards. For the fracture surfaces, the spectra obtained were of moderate quality

and the interference peaks were quite broad. However, the average thickness of oxide estimated for the fracture surface was within ±7% of that estimated for the normal surface for the same exposure condition.

No evidence for an acceleration or deceleration of corrosion was found inside the crevices of the incipient cracks. Similarly thicknesses measured in the weld-affected zone were comparable to those on the parent material of an incipient crack. The corrosion kinetics under the test conditions had been quite similar for the normal and fracture surfaces.

A good agreement was observed between the thicknesses estimated and those predicted by the kinetic equation reported in the literature (4). In the case of in situ fatigue corroded specimens, the difference in thickness between measurements at crack initiation and crack tip sites was the same as that predicted by the kinetic equation. The kinetics of oxide growth at crack initiation site (precracked at room temperature) had been comparable to that on a fresh metal surface exposed during the test (crack tip).

4. DATING DNGS ENDPLATE FRACTURES

4.1 Development of the DNGS Growth Equation

First attempts to model the cubic kinetics used the equation developed by Peters (4):

$$t = 250 * e^{-4062/kT} * d^{0.33}$$

where "t" is the oxide thickness and "d" the exposure time in days.

Because the oxide measurements made on DNGS out of flux endplates did not strictly follow Peters' equation, new Arrhenius constants were determined using averaged oxide thickness measurements from the upstream and downstream out of flux endplates.

By using the detailed operational history outlet temperatures were calculated. Because reactor data is reported in terms of inlet temperature and percent power, the outlet temperature was calculated as follows:

$T_{out}=T_{in}+(T_{out}-T_{in})x$ % Power; $T_{in}=265°C$, $T_{out}=310°C$(at 100% power)

From the reactor history and the measured average inlet and outlet thicknesses of 0.73 and 1.23 μm, Arrehenius constants were determined. The resulting growth equation is:

$$t = 1365 * e^{-5059/KT} * d^{0.33}$$

4.2 Using the DNGS Growth Equation to Determine Time of Failure

Figure 3 shows the combination of the detailed reactor history (ie, outlet temperature) along with the calculated endplate oxide thickness. The time axis is shown in both calendar days and accumulated days. Several growth curves are shown which result from starting the oxide growth (i.e., newly exposed fracture surface) at several different times during the reactor history cycle. If the fracture occurred prior to August 1990 the resulting oxide thickness 1.20 μm would be within experimental spread of 1.23 $\pm$ 0.05 μm observed on the normal surface. Thus all failures occurring before the reactor coming on line in August are rendered indistinguishable.

For the other three chosen fracture times, shown in Figure 3, well separated oxide thicknesses are observed; 0.93, 0.79 and 0.27 μm respectively. Figure 4 shows the construction of the failure estimation curve from oxide thicknesses, calculated for the various fracture times chosen. To construct the complete DNGS failure curve, the detailed history was simplified into 23 isothermal periods. The resulting failure curve (solid line marked outlet curve) can be used to predict failure times from oxide thickness measured on the fracture face for specimens having an "average" oxide thickness of 1.23 μm on the normal face.

To extend the fracture failure estimation curve to include the variation in average oxide thicknesses observed on the downstream (outlet) endplate, a range factor, k^1, is introduced into the growth equation.

$$t = k^1 * 1364 * e^{-5059/KT} * d^{0.33}$$

The k^1 factor for various calculated oxide thicknesses is shown in Table 1.

TABLE 1
ACCOMMODATING FOR NORMAL FACE OXIDE THICNESS VARIATION

THICKNESS	RANGE FACTOR	EQUIV. TEMP °C
1.09	0.85	300
1.15	0.94	305
1.23	1.00	310
1.31	1.07	315
1.39	1.13	320

Alternatively, the differences in the observed endplate oxide thicknesses can be described as a variation in the local temperature. Included in Table 1 are the equivalent temperatures if the stated thicknesses are a result of only thermal effects. The range of oxide thicknesses observed in DNGS (i.e., 1.11 to 1.34) would require a $\pm 7^{\circ}C$ temperature variation. Because both range factor and temperature variation result in multiplicative modification of the kinetic equation, they are equivalent in describing endplate oxide thickness variation for dating purposes. The range factor was most convenient and was used to develop a "family of failure curves".

The dashed lines in Figure 4 show the time to failure curves at 0.03 μm intervals; oxide thicknesses calculated at shutdown are plotted against Days From Shutdown (DFSD). These are used to obtain estimations of individual fracture times. The D2 K12/14 fracture time is shown as an example. The curve corresponding to the normal surface oxide thickness of the specimen, 1.17 μm is followed until the measured fracture oxide thickness, 1.03 μm, is reached. The corresponding time of fracture, July 31, 1990, is then obtained from the time axis. The scatter band along the time axis represents the limits in failure times based on maximum variability observed in the fracture oxide thickness measurement. The determined time of fracture uncertainty is dependent on both the variability in the oxide measurement as well as the slope of the normal surface curve to either side of the failure time. Because the spread is typically larger for the fracture face than for the corresponding normal oxide thickness, the spread introduced from uncertainty of the normal oxide thickness is ignored.

4.3 Results

Fractures were characterized into different confidence groups according to the size and quality of the collected spectra. A valid spectra was defined as having well defined peaks with minimal effects of absorption, dispersion, oxide non-uniformity and stray interference resulting from fatigue fracture features. The greater the number of valid spectra collected on a specimen the more confidence was placed in the failure time estimate.

TABLE 2
NUMBER OF VALID SPECTRA

Ranking	Normal Surface	Fracture Surface
Highest	>3	>5
Medium	2-3	3-5
Lowest	1-2	2-3

Specimen data meeting the above requirements are summarized in Table 3. On some fractures, two separate areas showed two thicknesses. These are identified A and B in Table 3. The results are plotted in Figure 5. The time axis has been expanded to the time period between June and December 1990 where fractures are observed. Highest, medium and lowest confidence results are identified appropriately. Exact identification of the points is possible using the results reported in Table 3.

TABLE 3
EXAMINED ENDPLATE FRACTURES

Specimen	Thickness FF/NF	No. of Pts. *FF	NF	Fracture Date	Uncertainty +Days	-Days
J13-1/26	1.04/1.34	4	4	Sept 11	10	22
J13-1/30A	0.87/1.19	4	8	Oct 05	3	4
J13-1/30B	0.50/1.19	2	8	Dec 04	2	2
R13-1/22A	1.29/1.34	7	10	June 20	11	6
R13-1/26A	1.23/1.34	4	8	July 16	9	6
R13-1/26B	1.14/1.34	4	8	Aug 10	6	18
R13-1/30	0.95/1.28	9	3	Oct 07	22	5
R13-1/22B	0.57/1.34	4	10	Dec 03	6	2
K12-1/26	1.26/1.33	2	3	July 06	16	12
K12-1/14	1.03/1.17	6	2	July 31	9	22
K12-1/30	1.02/1.19	2	1	Aug 08	7	7
K12/1/16	0.87/1.11	5	2	Sept 07	2	3
K12-1/12A	1.02/1.31	2	2	Sept 10	6	7
K12-1/12B	0.92/1.31	2	2	Oct 17	3	9
Q12-1/30	1.11/1.25	2	3	Aug 01	8	7
Q12-1/26	0.94/1.26	3	1	Oct 06	19	6

* FF - Fracture Face, NF - Normal Face

The lower confidence points suggest failure times close to those predicted by high confidence points that even the conditions of lowest confidence are sufficient to make relatively accurate failure estimates. Failures thus appear to occur in groups, rather than as individual events, throughout the power producing period of operation.

Uncertainty in the failure time prevents making confident associations with specific historical events. However, conditions during on-line operations are clearly necessary and sufficient to cause endplate failure.

5. CONCLUSIONS

Corrosion films on fracture and normal surfaces of endplates, from fuel bundles removed from Darlington Unit 2, varied in thickness from 0.5 to 1.5 microns. Infrared interferometry provided a nondestructive technique to accurately measure the thicknesses. An accuracy, relative to gravimetry, of ±5% was obtained by this technique.

Laboratory tests on fatigue-tested specimens showed that the kinetics of oxide growth on normal and fracture faces was the same. No evidence was found for a crevice corrosion effect in the incipient cracks and oxide thicknesses measured on the weld-affected zones of a crack were comparable to those on the parent material for the same exposure.

A method has been developed using oxide thicknesses from FTIR interferometry to accurately date fuel bundle endplate failures for the DNGS reactor. Endplate failure was not a single event. Failures occurred throughout the power producing period between July and December 1990. There are indications that failures occurred in groups at several periods during power production. Uncertainty in failure estimates prevent making associations with specific historical events. Lowest confidence data follow the same trend as more confident data.

6. REFERENCES

(1) RAMASUBRAMANIAN, N. AND SCHANKULA, M.H., "An Investigation of Waterside Corrosion of Fuel Cladding in CANDU Reactors Using Infrared Reflection Absorption Spectroscopy", Proc. Fifth International Symposium on Environmental Degradation of Materials in Nuclear Power Systems - Water Reactors, American Nuclear Society, p.•105-155, August 1991.

(2) WANKLYN, J.N., "The Properties of Oxide Films on Zirconium Alloys and Their Relevance to Corrosion and Hydrogen Uptake", Electrochemical Technology, 4, p.•81-88, 1966.

(3) WILKINS, N.J.M., "Optical Measurement of Oxide Films on Zirconium in the Range of Wavelengths from 2000 Å to 2.5 μm", Corrosion Science, 5, p. 3-18, 1965.

(4) PETERS, H.R., "Improved Characterization of Aqueous Corrosion Kinetics of Zircaloy-4", ASTM STP 824, p.·507-518, 1984.

ACKNOWLEDGEMENTS

Many people have contributed to this work: FTIR Spectra Collection, CRL-Victor Ling, Bernie Leger, Bernie Surrette, and W.S.-Leon Clegg; Data Interpretation Assistance: Bob Hosbons, Mark Floyd and Terry Carter; FTIR Calibration Methods: F. Amouzouvi and C.B. So; Specimen Preparation: J. Kelm and B. Stuthers; Laboratory Tests and FTIR Measurements: L. Chee, OHRD and DNGS Investigation Committee: E. Price, P. Truant, J. Juda, W. Stewart, M. Leger and M. Durand. We acknowledge the permission of Ontario Hydro and the DNGS committee to present this work.

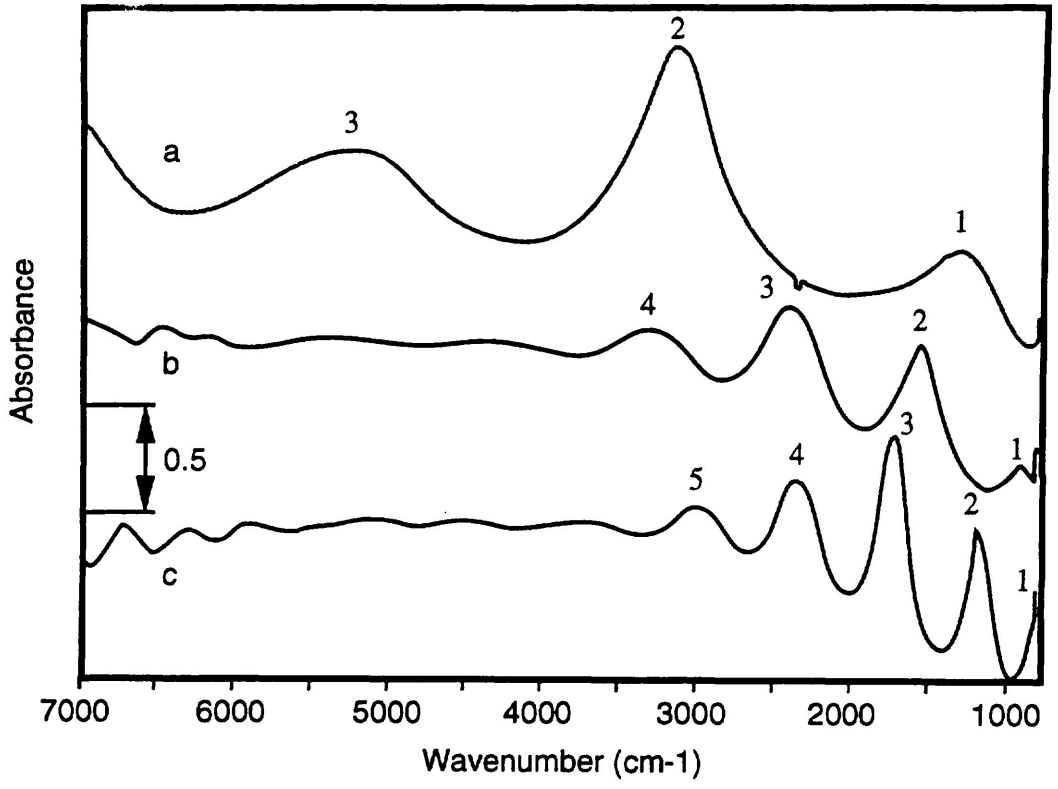

Figure 1. Interference spectra of corrosion film standards; (a) 1.2, (b) 2.77 and (c) 4.03 μm oxide growth on Zircaloy-4 fuel cladding.

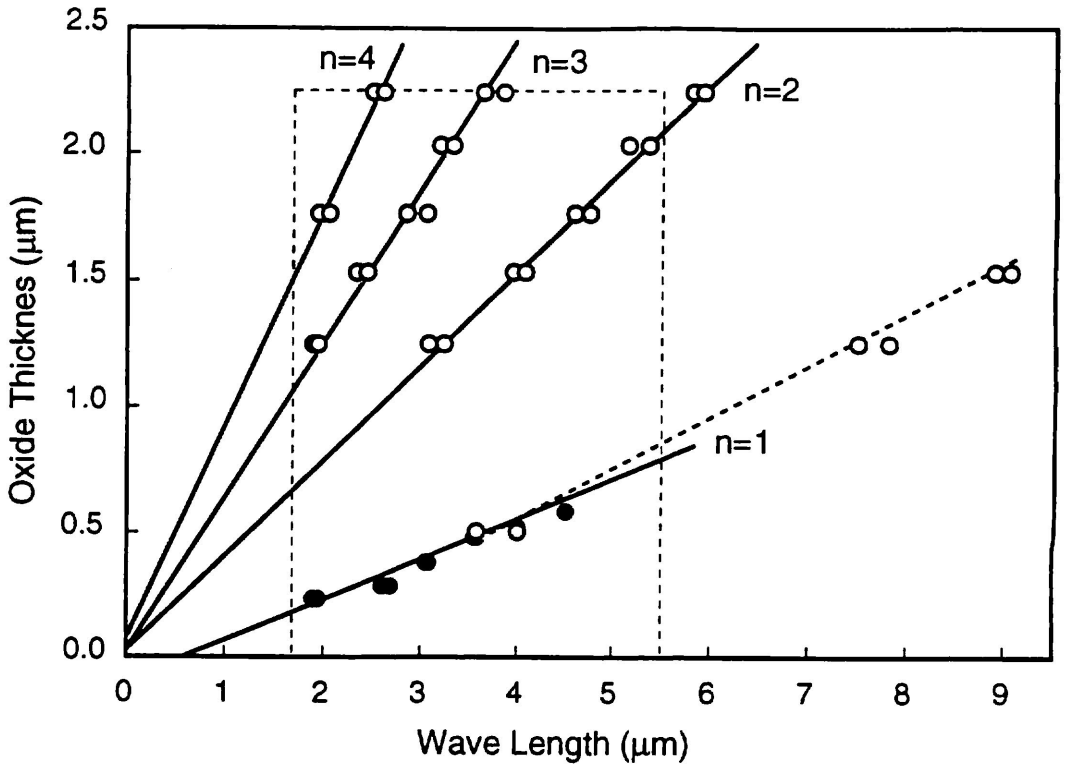

Figure 2. Oxide thickness vs. wavelengths of reflectivity minima for corrosion film standards on Zircaloy-4 cladding material; orders of interference n=1 to 4; O and ● thermal and anodic oxide films.

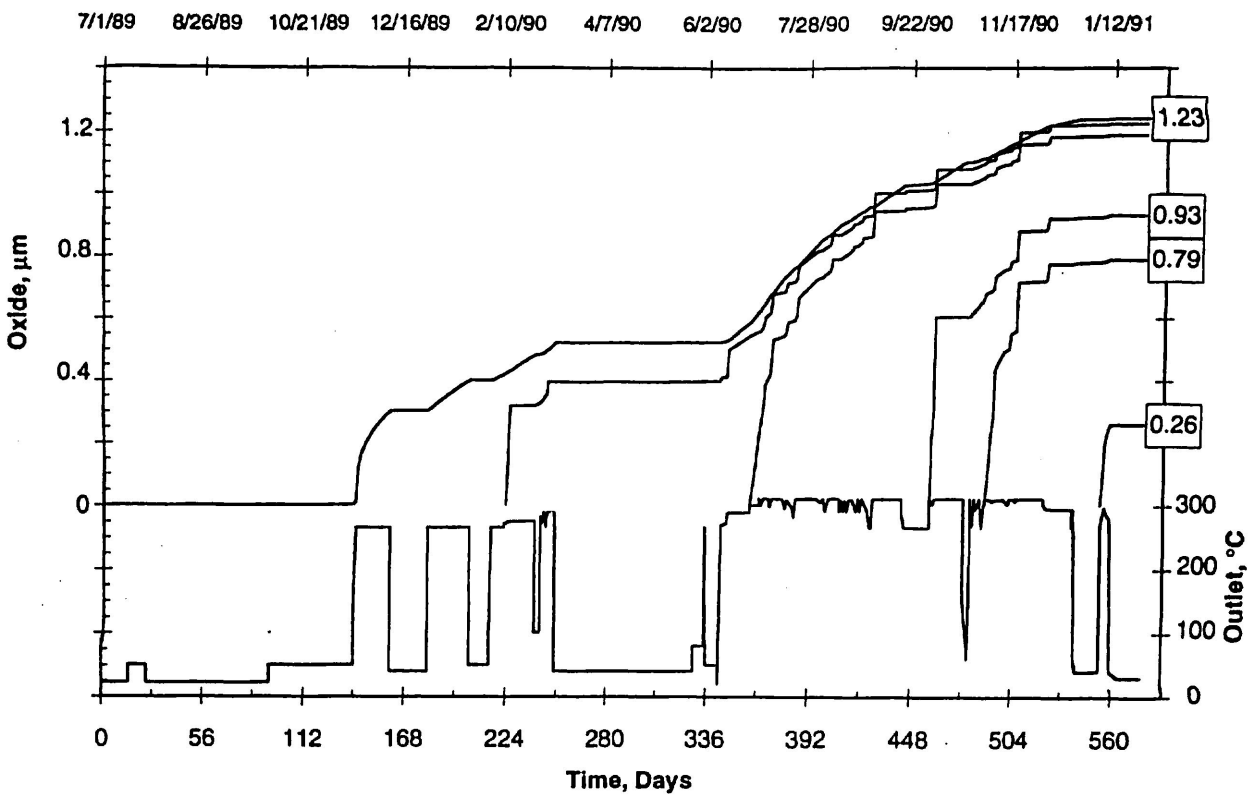

Figure 3. Kinetics of oxide growth on downstream endplate of bundle in position one in DNGS Unit #2.

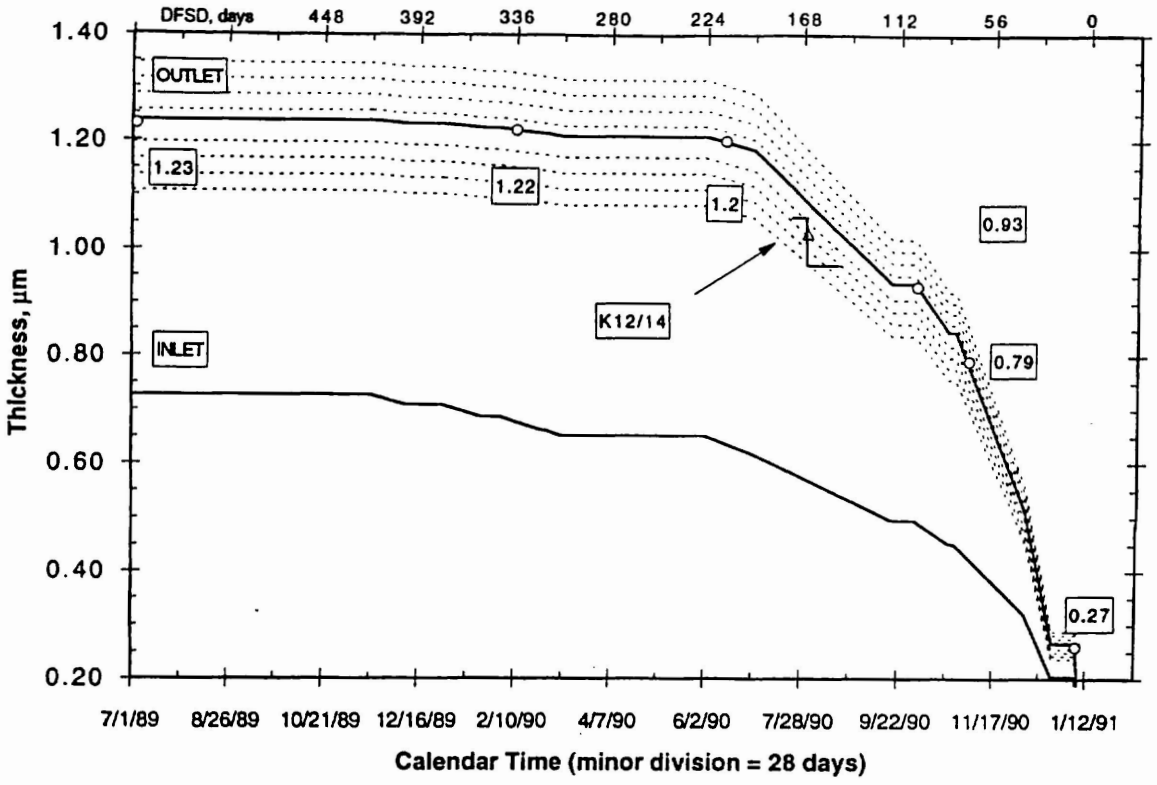

Figure 4. Failure time estimation curves calculated for oxide growth on downstream endplate of bundle in position one in DNGS Unit #2; oxide growth on normal face covers the range of thickness 1.1 to 1.35 µm.

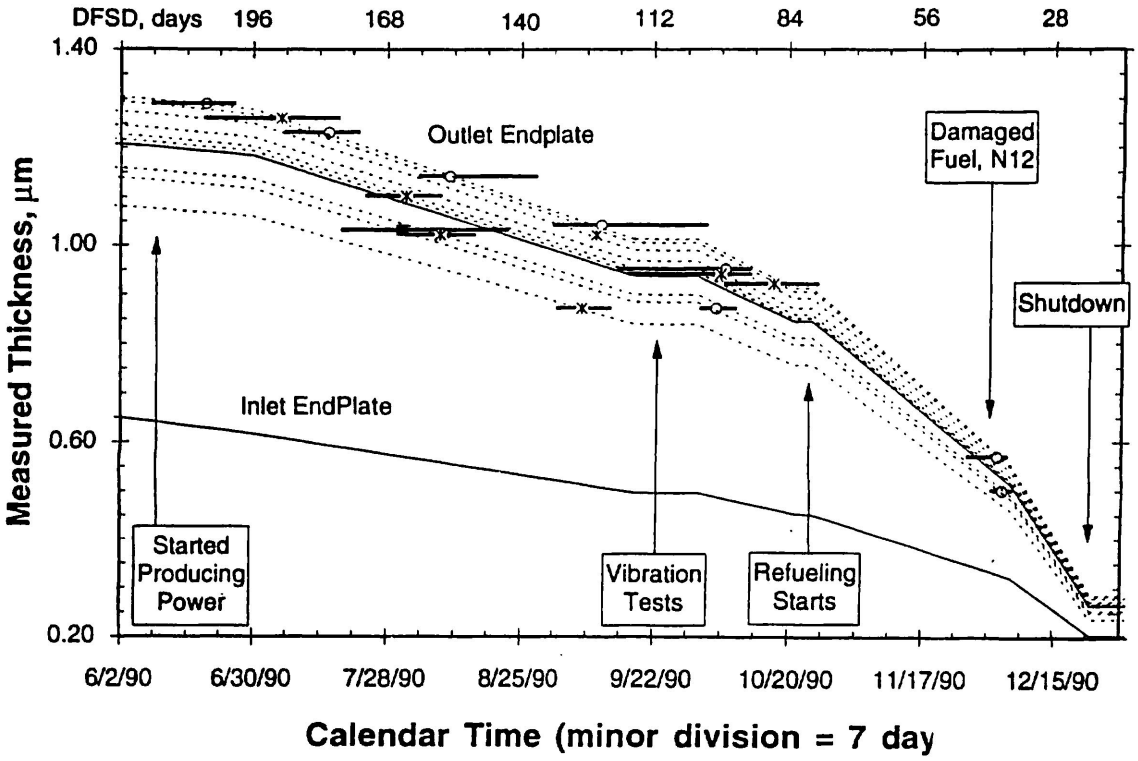

Figure 5. Failure dates for fractures observed on downstream endplates of bundles in position one in DNGS Unit #2; O - high confidence, ■ - medium confidence and X - low confidence data.